THE JOURNAL OF PHYSICAL CHEMISTRY C

Article

Cite This: J. Phys. Chem. C 2018, 122, 4809−4816

pubs.acs.org/JPCC

Charge Carrier Dynamics in $Cs_2AgBiBr_6$ Double Perovskite

Davide Bartesaghi,[†,‡,*] Adam H. Slavney,[§] María C. Gélvez-Rueda,[†] Bridget A. Connor,[§] Ferdinand C. Grozema,[†] Hemamala I. Karunadasa,[§] and Tom J. Savenije[†,*]

[†]Department of Chemical Engineering, Delft University of Technology, 2628CD Delft, The Netherlands

[‡]Materials Innovation Institute (M2i), 2628CD Delft, The Netherlands

[§]Department of Chemistry, Stanford University, Stanford, California 94305, United States

Supporting Information

ABSTRACT: Double perovskites, comprising two different cations, are potential nontoxic alternatives to lead halide perovskites. Here, we characterized thin films and crystals of $Cs_2AgBiBr_6$ by time-resolved microwave conductance (TRMC), which probes formation and decay of mobile charges upon pulsed irradiation. Optical excitation of films results in the formation of charges with a yield times mobility product, $\varphi\Sigma\mu > 1$ cm^2/Vs. On excitation of millimeter-sized crystals, the TRMC signals show, apart from a fast decay, a long-lived tail. Interestingly, this tail is dominant when exciting close to the bandgap, implying the presence of mobile charges with microsecond lifetimes. From the temperature and intensity dependence of the TRMC signals, we deduce a shallow trap state density of around $10^{16}/cm^3$ in the bulk of the crystal. Despite this high concentration, trap-assisted recombination of charges in the bulk appears to be slow, which is promising for photovoltaic applications.

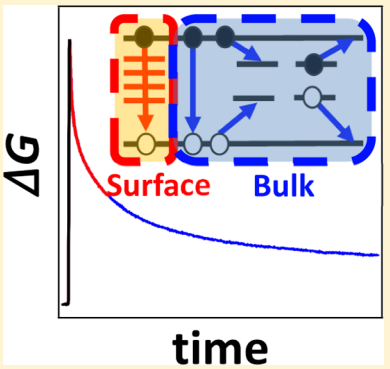

INTRODUCTION

Metal halide perovskites ($APbX_3$; with A = $CH_3NH_3^+$, $(H_2N)_2CH^+$, or Cs^+ and X = I^-, Br^-, or Cl^-) have recently attracted much attention because of their applicability as highly efficient solar cell absorber layers for thin film photovoltaics. The increasing interest in perovskite solar cells is motivated by the fast rise of their power conversion efficiency over less than a decade, from less than 4%[1] to more than 22%.[2] The attractiveness of metal-halide perovskites would further benefit from the replacement of Pb^{2+} with a nontoxic alternative;[3] however, experimental and theoretical results have so far shown that homovalent substitution of lead (e.g. with Sn^{2+}) has a negative effect on the optoelectronic properties and the stability of metal-halide perovskites.[4−11]

Recently, attention has been given to quaternary $A_2B'B''X_6$ double perovskites, in which neighboring B′ and B″ sites in the lattice are occupied by alternating mono- and trivalent metal cations.[12] Several publications reported the synthesis and characterization of the double perovskites $Cs_2AgBiBr_6$,[13,14] which has an indirect bandgap in the range 1.95−2.19 eV.[13−18] Besides application in photovoltaic devices,[20] it has been shown that $Cs_2AgBiBr_6$ can be used to fabricate X-ray detectors with a low detection limit.[21] More recently, some of us reported the synthesis and characterization of an analogous double perovskite alloyed with a small percentage of Tl, yielding $Cs_2(Ag_{1-a}Bi_{1-b})Tl_xBr_6$ ($x = a + b$) crystals. With respect to pristine $Cs_2AgBiBr_6$, the Tl-alloyed $x = 0.075$ material has a much smaller bandgap of ca. 1.5 eV, which makes it potentially applicable in single junction solar cells.[19]

Time-resolved photoluminescence (TRPL) measurements on $Cs_2AgBiBr_6$[14] crystals and powder show a rapid initial decay with at least some of the charges recombining on a nanosecond timescale. On the other hand, the tail of the TRPL traces reported in ref 14 has a lifetime comparable to that of optimized lead halide perovskite films,[22,23] which motivates the interest in this material as a possible absorber in solar cells. The weak PL intensity measured for $Cs_2AgBiBr_6$ suggests that the dominant recombination mechanism in this material is nonradiative, which is consistent with the indirect nature of the bandgap. Thus, further investigation of the charge carrier dynamics employing techniques complementary to TRPL can provide a more complete picture of the recombination processes in $Cs_2AgBiBr_6$.

In this paper, we present an in-depth study on the charge carrier dynamics in $Cs_2AgBiBr_6$ single crystals and films, measured by means of the time-resolved microwave conductance (TRMC) technique.[24] This technique probes the generation and decay of the mobile charges generated upon pulsed irradiation. First, we measured the temperature-dependent optical properties of $Cs_2AgBiBr_6$ thin films. Next, we recorded the photo-induced TRMC signals of these films, from which we determined the charge mobility. Subsequently, we studied the $Cs_2AgBiBr_6$ crystals in more detail by measuring the temperature- and intensity-dependent photo-induced TRMC traces at different wavelengths. Additionally, we performed complementary pulse-radiolysis TRMC (PR-TRMC) measurements in which charges are generated by a short pulse of high-energy electrons. This results in the generation of a uniform

Received: January 17, 2018
Revised: February 1, 2018
Published: February 5, 2018

DOI: 10.1021/acs.jpcc.8b00572
J. Phys. Chem. C 2018, 122, 4809−4816

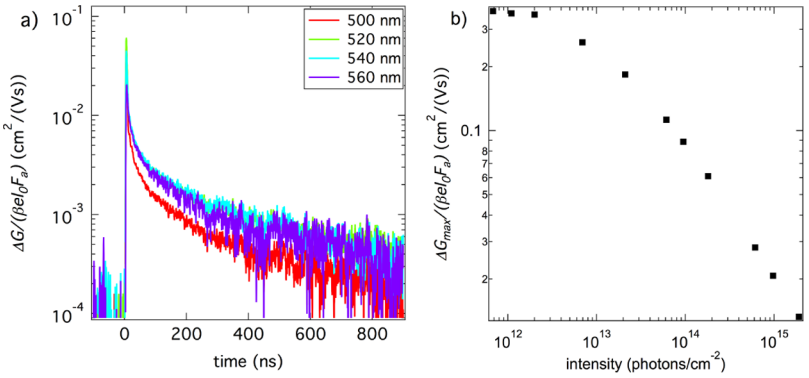

Figure 1. (a) TRMC traces for a $Cs_2AgBiBr_6$ thin film recorded upon pulsed laser excitation in the wavelength range 500−560 nm at room temperature. The photoconductance, ΔG is normalized for the number of incident photons ($I_0 \approx 2.0 \times 10^{15}$ cm^{-2}) and for the fraction of absorbed photons (F_a); (b) maximum photoconductance vs photon fluence upon optical excitation at 500 nm.

concentration of free electrons and holes whose mobility can be determined as a function of temperature.[25−27] Finally, we combined all the information obtained from both TRMC and PR-TRMC measurements into a comprehensive kinetic model for the generation, trapping, and recombination of charges in $Cs_2AgBiBr_6$.

METHODS

Crystal Synthesis. Single crystals of $Cs_2AgBiBr_6$ and $Cs_2(Ag_{1-a}Bi_{1-b})Tl_xBr_6$ (x = 0.075) were synthesized following the procedure reported in ref 14 and in ref 20, respectively.

Preparation of Thin Films. Stoichiometric quantities of $BiBr_3$ (74 mg, 0.17 mmol), AgBr (32 mg, 0.17 mmol), and CsBr (62 mg, 0.34 mmol) were combined in DMSO (330 μL). The mixture was heated to 100 °C under stirring, and the solids dissolved yielding a yellow solution. The hot solution (25 μL, still at 100 °C) was deposited on a glass or fused silica substrate (2.1 cm^2) and spun at 500 rpm for 30 s (acceleration of 100 rpm/s) and then at 5000 rpm for 45 s (acceleration of 4000 rpm/s). During the second spinning step, dry air was blown gently into the top of the spin-coater to accelerate solvent evaporation. Immediately after spinning was complete, the film was annealed in air at 200 °C for 5 min.

Optical Characterization. $Cs_2AgBiBr_6$ thin films were mounted in a liquid nitrogen cryostat and placed in a Lambda 900 UV−vis spectrometer (PerkinElmer) for temperature-dependent transmittance measurements. The measurement was conducted in a nitrogen atmosphere. The room temperature reflectance was acquired in air using a Lambda 1050 UV−vis spectrometer (PerkinElmer).

Photo-Induced Time-Resolved Microwave Conductance Measurements. A small number of $Cs_2AgBiBr_6$ or $Cs_2(Ag_{1-a}Bi_{1-b})Tl_xBr_6$ (x = 0.075) crystals were glued to a quartz substrate and mounted in a microwave cell, which was sealed within a nitrogen-filled glovebox. The TRMC technique was used to measure the change in microwave (f = 8.5 GHz) power after pulsed optical excitation (repetition rate: 10 Hz). The rise of $\Delta P/P$ is limited by the response time of the microwave system and by the width of the laser pulses (3.5 ns). Light intensity dependence was measured by varying the intensity of the incident laser pulses with a series of neutral density filters.

Pulse-Radiolysis Time-Resolved Microwave Conductance. Crystals of $Cs_2AgBiBr_6$ were placed in a polyether ether ketone (Peek) sample holder and sealed with PMMA dissolved in chlorobenzene (13 mg/mL) within a nitrogen-filled glovebox, before mounting in the microwave cell. PR-TRMC was used to measure the mobility and temporal decay of conductivity of free charge carriers in $Cs_2AgBiBr_6$. The free charge carriers are generated using a high energy electron pulse (3 MeV with a pulse length varying between 0.2 and 2 ns). The effective ionization energy (~20 eV) assures that the carriers are generated far away from each other without damaging the sample from radiation exposure. The radiation dose used is ~8 × 10^6 W/cm^3, 3 orders of magnitude lower than radiation doses that provoke damage to perovskite samples.[28] The concentration of charge carriers generated was varied between 1 × 10^{15} and 2 × 10^{16} cm^{-3}, depending on the length of the pulse. The thermal relaxations of the charges that are produced in this way occurs well within a nanosecond, and hence it does not influence the recombination of the charges. After excitation, the temporal decay of conductivity due to mobile charge carriers is determined from the measured change in microwave power (f = 28−38 GHz). The response time of the PR-TRMC is 1 ns. The microwave cell is contained in a cryostat in which the temperature can be varied between −150 and 200 °C. The temperature was maintained for ~15 min before doing the measurement to assure the equilibrium of the system.

RESULTS AND DISCUSSION

Thin films and millimeter-size crystals of $Cs_2AgBiBr_6$ were synthesized and characterized using the methods briefly described in the Methods Section and reported previously.[14] First, we performed temperature-dependent transmittance measurements (90−300 K) on $Cs_2AgBiBr_6$ films, which were corrected using the reflection spectra recorded at room temperature. From the Tauc plot, assuming an indirect allowed transition (Figure S1), an almost temperature-independent bandgap of 2.02 ± 0.02 eV is derived, which is in agreement with previous reports.[13−18] The nearly temperature-independent absorption data do not suggest substantial contribution of any excitonic transition on lowering the temperature.

Next, the films were mounted in a TRMC cell and excited between 500 nm (2.48 eV) and 600 nm (2.07 eV), thus probing the charge dynamics for excitation well above or close to the optical bandgap of $Cs_2AgBiBr_6$. The photoinduced TRMC technique measures the change in photoconductance (ΔG) as a function of time on optical excitation of the sample.[24] Immediately on excitation, ΔG sharply rises as a result of the photogeneration of mobile charge carriers, which is

DOI: 10.1021/acs.jpcc.8b00572
J. Phys. Chem. C 2018, 122, 4809−4816

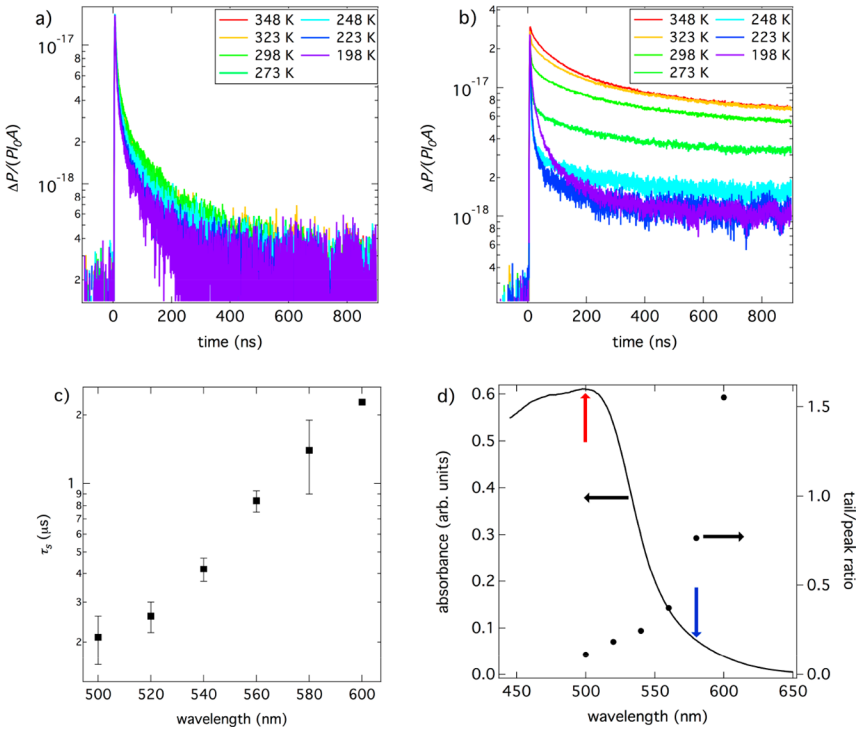

Figure 2. (a,b) TRMC traces for $Cs_2AgBiBr_6$ crystals recorded upon pulsed laser excitation at 500 (a) and 580 nm (b) at indicated temperatures. The fraction of absorbed microwave power $\Delta P/P$ is normalized for the number of incident photons ($I_0 \approx 1.1 \times 10^{15}$ cm^{-2}) and for the surface area of the sample ($A \approx 0.12$ cm^2); (c) decay constant of the slow component of the room temperature TRMC traces measured upon pulsed laser excitation at different wavelengths; (d) absorbance spectrum of $Cs_2AgBiBr_6$ (solid line) and the tail/peak ratio of the TRMC traces measured upon pulsed laser excitation at different wavelengths, with incident photon fluence $I_0 \approx 1.1 \times 10^{15}$ cm^{-2} (dots). The red and blue arrows indicate the absorbance at 500 and 580 nm, respectively. Details about the double exponential fitting from which the tail/peak ratio has been determined are shown in the Supporting Information. The absorption data have been taken from ref 14.

followed by a decay due to charge recombination and/or immobilization of carriers in trap states within the bandgap. To compare TRMC signals collected at different wavelengths, ΔG is normalized for the number of incident photons (I_0) and for the fraction of absorbed light (F_a).

The ΔG transients measured for a 400 nm thick film of $Cs_2AgBiBr_6$ upon optical excitation at different wavelengths are shown in Figure 1a. The decay of the TRMC signals is slightly slower for excitation at longer wavelengths. If no charge carrier recombination takes place on the timescale of the response time of the setup (3.5 ns), the product of the charge photogeneration yield, φ and the sum of electron and hole mobility $\Sigma\mu$ is directly proportional to the maximum photoconductance (ΔG_{max})[24]

$$\varphi \sum \mu = \frac{\Delta G_{max}}{\beta e I_0 F_a} \quad (1)$$

where β is the ratio of the inner dimensions of the microwave cell, and e is the elementary charge. In Figure 1b, the $\varphi\Sigma\mu$ product is plotted as a function of the photon fluence for optical excitation at 500 nm. For a photon fluence beyond 1.1 $\times$ 10^{12} cm^{-2}, $\varphi\Sigma\mu$ decreases, which we attribute to fast recombination of charges during the laser pulse. The slope of $\log(\varphi\Sigma\mu)$ versus $\log(I_0)$ is close to $-1/2$, which implies a dominant bimolecular decay process such as band-to-band recombination.[24] For lower photon fluences, $\varphi\Sigma\mu$ is virtually independent of I_0 and amounts to 1.1 cm^2 V^{-1} s^{-1}. In view of the absence of excitonic features in the optical absorption, we assume φ to be close to 1. However, as will be argued later, fast charge decay by sub-nanosecond trapping or recombination occurring within the response time of our instrument may limit φ. Hence, the lower bound of the mobility in $Cs_2AgBiBr_6$ is 1 cm^2 V^{-1} s^{-1}, an order of magnitude lower than the value commonly reported for lead halide perovskites.[29] Recently, Tang et al. measured a charge mobility of 11.81 cm^2 V^{-1} s^{-1} in $Cs_2AgBiBr_6$ single crystals by space charge limited current methods.[21] The lower values measured in this work can be explained by the fact that the charge transport properties are typically superior in single crystals.[29]

In Figure 2a,b, the TRMC traces measured for $Cs_2AgBiBr_6$ single crystals at different temperatures for excitation at 500 and 580 nm are shown. For crystals, the TRMC results are expressed as ($\Delta P/P$) as a function of time, normalized for I_0 and for the surface area of the sample (A). Comparable to what has been observed in ref 14 by means of TRPL, the TRMC signals show a rapid initial decay and a slow tail, which is more evident at longer excitation wavelengths. As shown in Figure S2 in the Supporting Information, the signal measured on excitation at 580 nm has not fully decayed within 8 μs after optical excitation. These lifetimes are in the same order of magnitude as those previously found in single crystals of $CH_3NH_3PbI_3$.[30] The TRMC traces recorded upon pulsed excitation at other wavelengths are reported in Figure S3 in the Supporting Information; the data have been fitted with a double exponential function

$$y(t) = A_f \exp\left(-\frac{t}{\tau_f}\right) + A_s \exp\left(-\frac{t}{\tau_s}\right) \quad (2)$$

DOI: 10.1021/acs.jpcc.8b00572
J. Phys. Chem. C 2018, 122, 4809−4816

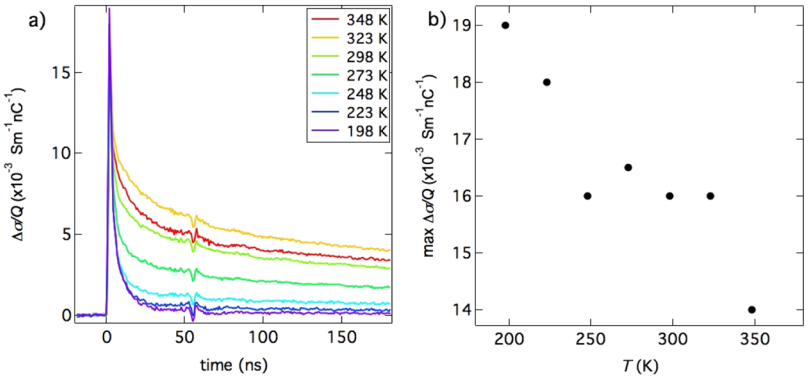

Figure 3. (a) PR-TRMC traces at different temperatures for $Cs_2AgBiBr_6$ crystals. The duration of the electron pulse was 1 ns; (b) maxima in the PR-TRMC traces plotted against the temperature.

where τ_f and τ_s are the decay constants of the fast and slow components of the traces, respectively. A plot of τ_s versus the wavelength (Figure 2c) shows a clear increase in values above 1 μs with longer wavelengths. The ratio of the coefficients A_s and A_f (tail/peak ratio) is shown in Figure 2d together with the absorption spectrum of polycrystalline $Cs_2AgBiBr_6$.[14] This ratio provides a measure of the fraction of charges decaying via a slow pathway. The rise of the long-lived tail occurs at the same wavelength range in which the absorption is rapidly decreasing, that is, the penetration depth of light into the crystal is increasing. From the measured absorption coefficient (Figure S1e), we calculated a penetration depth in the range of 170–190 nm for an excitation wavelength of 500 nm. Increasing the excitation wavelength to 580 nm results in a penetration depth of more than 5 μm. Thus, we assign the long-lived tail to mobile charges generated deep in the bulk of the crystal, while we attribute the fast decay to surface-related recombination. Fast surface recombination causes the depletion of mobile charges in the vicinity of the surface; this results in a concentration gradient that leads to the diffusion of charges from the bulk of the film toward the surface. For excitation at 500 nm, most of the charges are generated within 170 nm from the surface, which diffuse toward the surface and recombine within a few nanoseconds. Charges generated deeper in the bulk using longer excitation wavelengths escape from surface recombination, giving rise to the long-lived tail in the TRMC signals.

In the thin film samples, the long-lived tail is almost absent (Figure S4), indicating that charge dynamics in the 150 nm $Cs_2AgBiBr_6$ films are mostly dominated by surface effects. However, second-order band-to-band recombination is also active. In fact, the normalized TRMC traces for the thin film excited at 500 nm are decaying faster at higher photon fluences (Figure S5).

To obtain more knowledge regarding the mechanisms controlling the charge dynamics in bulk $Cs_2AgBiBr_6$, we performed temperature- and intensity-dependent TRMC measurements on millimetre-size crystals. As shown in Figure 2a,b, the TRMC traces upon excitation at 500 nm are almost independent of the temperature, whereas for the traces recorded at 580 nm, changing the temperature affects both the size and the lifetime of the traces. The maximum TRMC signal magnitude decreases somewhat upon lowering the temperature from 348 to 248 K and rises again upon further cooling (Figure S6). Surprisingly, the relative contribution of the long-lived tail is completely suppressed upon cooling down to 198 K (Figures 2b and S6). We note that upon further cooling to 123 K, the tail rises again (Figure S7). We limit our discussion in the remainder of the paper to the temperature range 198–348 K. The TRMC signal is proportional to the concentration of both charge carriers and to the sum of their mobilities ($\Sigma\mu$). Hence, a possible explanation for the suppression of the tail is that the mobility decreases at lower temperatures, although this would be in contrast with previous reports on lead-based perovskites.[31−33]

To reveal how the mobility varies with temperature, we performed PR-TRMC measurements in which a short high-energy electron pulse leads to the generation of charges with a uniform low concentration profile over the whole crystal.[25−27] The charge carrier yield in a PR-TRMC experiment is only dependent on the density and on the bandgap of the sample and does not vary with temperature. Thus, the temperature dependence of the maximum change in radiation-induced conductivity corresponds directly to the temperature dependence of $\Sigma\mu$. PR-TRMC traces for $Cs_2AgBiBr_6$ are shown in Figure 3a for temperatures varying from 198 to 348 K. The decays are very similar to those measured by laser excitation at 580 nm, showing a very fast decay back to zero at low temperatures, whereas at higher temperatures, a long-lived tail is clearly observed. The maximum change in radiation-induced conductivity is plotted versus temperature in Figure 3b. A clear increase in the maximum change in conductivity, and hence in $\Sigma\mu$, is observed with lower temperatures. Analogous to lead-perovskites,[27,31−33] this dependence can be attributed to a reduction in phonon scattering at low temperatures, which is typical for the band-like transport.

From the above PR-TRMC measurements, we conclude that $\Sigma\mu$ monotonically increases upon cooling and hence the suppression of the tail of the light-induced TRMC signal measured upon excitation at 580 nm (Figure S6) cannot be explained by lowering mobilities. Also a substantial reduction of the absorption coefficient or a blue shift of the onset of the absorption spectrum can be discarded as the possible explanation for the disappearance of the tail in view of the nearly temperature-independent thin film spectra (Figure S1a,b). Hence, the reduction of the peak height from 348 to 248 K is most likely due to a decrease in the photogeneration yield φ and/or to rapid recombination or immobilization of charges faster than the time resolution of our experiment at lower temperatures. As argued above, we exclude substantial exciton formation in $Cs_2AgBiBr_6$ in the studied temperature range. This implies that φ is independent of temperature and

DOI: 10.1021/acs.jpcc.8b00572
J. Phys. Chem. C 2018, 122, 4809−4816

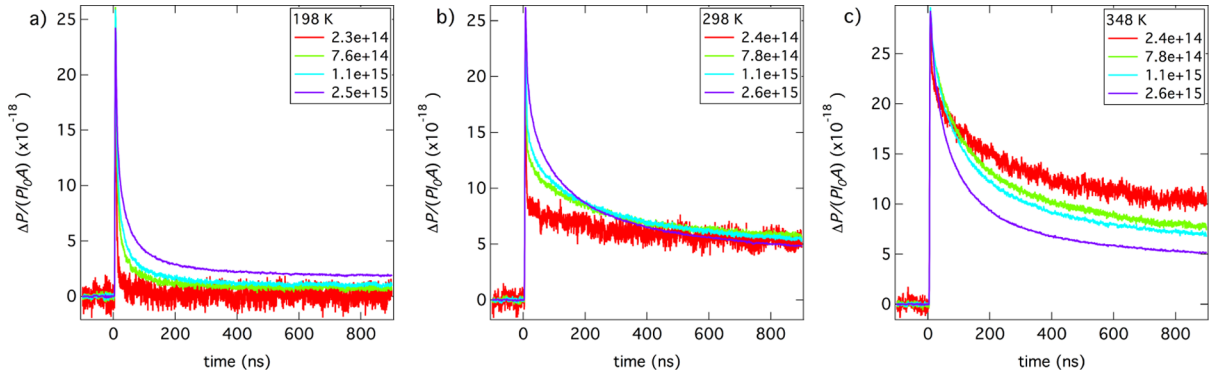

Figure 4. TRMC traces recorded at different photon fluences for $Cs_2AgBiBr_6$ single crystals upon pulsed laser excitation (λ = 580 nm) at 198 (a), 298 (b), and 348 K (c). The values of the photon fluence in the legends are expressed in photons/cm^2.

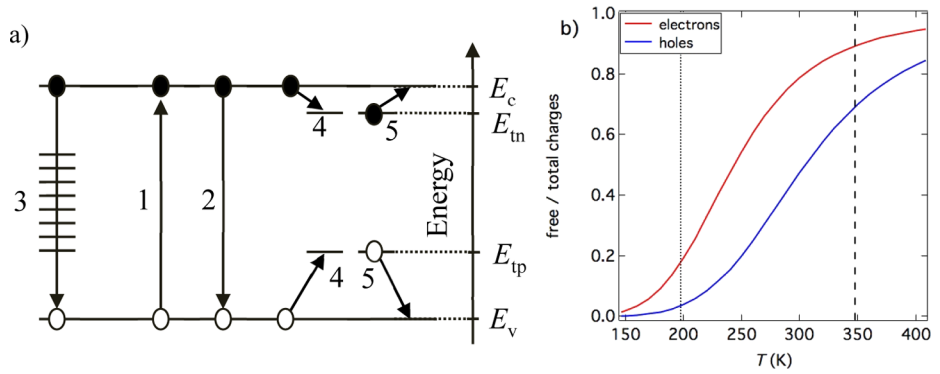

Figure 5. (a) Schematic representation of the band structure of $Cs_2AgBiBr_6$. Upon absorption of laser pulse, free electrons and holes are generated (1) in the conduction (E_c) and valence band (E_v), respectively. Subsequently, charges can recombine via band-to-band recombination (2) or via surface states (3). In the bulk of the material, shallow electron traps (at the energy level E_{tn}) and hole traps (at the energy level E_{tp}) are present. Free charges can be captured by these trap states (4), whereas trapped charges can be thermally released to the band edges (5). (b) Equilibrium distribution of electrons and holes represented as the ratio of the number of free charges to the total number of charges (free + trapped). The dashed and dotted lines represent experimental conditions for Figure 4a,c, respectively. The two distributions have been calculated using the Fermi distribution function, assuming that the energy level of the hole traps lies deeper in the bandgap with respect to the energy level for the electron traps (assuming the opposite would not change our argument). See the Supporting Information for details on the calculation.

that the temperature dependence of the TRMC signals is mainly governed by additional fast nanosecond recombination or trapping of charges at lower temperatures. The similarity of the PR-TRMC and TRMC recorded at various temperatures is in line with this explanation.

To obtain more knowledge of the mechanism which controls the decay of charges, we show in Figure 4, the intensity-normalized TRMC traces for $Cs_2AgBiBr_6$ recorded at 198, 298 and 348 K upon optical excitation at 580 nm. At 348 K, increasing I_0 results in a faster decay of the TRMC signals. At 198 K, the intensity dependence is the opposite: a long-lived tail is observable only at high I_0. The transition between the two different intensity dependencies is gradual; at intermediate temperatures, the TRMC signals show almost no dependence on I_0 (Figure 4b). These findings suggest that at different temperatures, the recombination of charges is dominated by different processes. Intensity-dependent TRMC traces for other intermediate temperatures are reported in the Supporting Information (Figure S8).

On the basis of the above results, we propose a kinetic model for carrier recombination in $Cs_2AgBiBr_6$ as summarized in Figure 5a. Because of the high absorption coefficient of the material well above the bandgap, excitation at those wavelengths implies that all the charge carriers are generated relatively close to the surface. Apart from surface recombination, the fast decay observed could in part be due to the occurrence of bimolecular or Auger recombination, as suggested from the intensity dependence of the thin film TRMC signals (Figure 1b). To obtain more insight, we repeated the TRMC measurements after grinding the $Cs_2AgBiBr_6$ crystals to obtain a micrometer-sized powder (Figure S9). Such powder shows a powder X-ray diffraction pattern identical to the one calculated using the crystallographic data and to the one measured for the thin film (Figure S10). Within the micrometer-sized powder, all the charges are generated relatively close to a surface, regardless of the penetration depth of the exciting radiation. Thus, diffusion toward the surface rapidly occurs and the photogenerated charges decay via surface recombination. For this reason, the TRMC traces recorded for the powder at any excitation wavelength, even at 580 nm, decay within a few nanoseconds. Hence, we conclude that for the crystal the decay for photoinduced carriers generated within hundreds of nanometers of the surface proceeds via surface recombination. At longer excitation wavelengths, more charges are generated in the bulk of the sample, and the fraction of carriers lost to surface recombination is thus smaller.

Temperature- and intensity-dependent TRMC traces provide the additional information about the recombination processes in the bulk. The intensity dependence at high temperature

DOI: 10.1021/acs.jpcc.8b00572
J. Phys. Chem. C 2018, 122, 4809−4816

(signal size decreasing with higher laser fluences) is typical of higher-order recombination processes, for example, bimolecular band-to-band recombination of free charges or Auger recombination.[34] In contrast, the opposite intensity dependence observed at low temperature is a signature of charge trapping: at low fluence, all the photogenerated charges are captured by trap states, while saturation of traps at higher fluence leaves some mobile charge carriers in the conduction and valence bands. Thus, the suppression of the long-lived tail upon cooling is assigned to the immobilization of charges in shallow trap states.

On the basis of our data, we can make a few statements about the traps in $Cs_2AgBiBr_6$. First, for optical excitation at 580 nm, we can approximate the generation profile as constant throughout the crystal and calculate the density of excess charge carriers generated in the bulk. At the highest laser fluences of our experiment, we do not observe higher-order recombination at low temperature, which means that even at the highest fluences most of the charges are trapped and the density of free charges is low. A high I_0, corresponding to a charge density of ca. 10^{16} cm^{-3}, is necessary to observe a long-lived tail at 198 K; we therefore suggest that the upper limit for the density of traps in the bulk of the material is in the order of 10^{16} cm^{-3}, which is 3 orders of magnitude higher than the value proposed for lead-based perovskite single crystals.[30] The temperature-assisted release of trapped charges back to the band does not require high activation energies; already at 348 K ($k_BT \approx 30$ meV), the intensity-dependent TRMC traces show second-order kinetics. This is an indication of shallow trapping, with trap states lying only a few tens of million electronvolts away from the band edges.

Assuming that the hole trap states are close to the valence band, at low temperatures and low laser intensities, we would have complete immobilization of holes. The presence of mobile electrons in the conduction band would still be detected by TRMC. However, the measurements performed at low temperature and low laser fluence do not show a long-lived tail. This might have two possible origins. The first option is that there is a large asymmetry between the mobilities for electrons and holes. On the basis of the limited difference (less than a factor 3) between the calculated effective masses for electrons and holes reported in the literature,[13,15] we discard this explanation. Therefore, we propose that there are both electron and hole traps present in the bulk of the crystal. Hence, at low temperatures and low excitation intensities, both electrons and holes are trapped (Figure 5b). At higher temperatures, a substantial part of both the trapped electrons and holes are thermally released. The nature of such trap states remains unknown; calculations have suggested that point defects such as silver vacancies and silver-on-bismuth antisites have low formation enthalpies and may act as electron or hole traps because of their energy levels in the bandgap.[17] Future work will aim at determining the nature, the density and the position of the charge traps within the bandgap of $Cs_2AgBiBr_6$.

Finally, we note that TRMC measurements for $Cs_2(Ag_{1-a}Bi_{1-b})Tl_xBr_6$ ($x = a + b = 0.075$) yield similar results as in the case of the pristine material: a fast decay on the nanosecond scale for optical excitation at an energy well above the bandgap is observed, while upon increasing the excitation wavelength, a tail is visible (Figure S11). The temperature dependence of the long-lived tail is also similar to that observed for the pristine double perovskite. However, it was not possible to measure the intensity dependence of the tail because of the limited size of the crystals.

CONCLUSIONS

From TRMC measurements on the double perovskite $Cs_2AgBiBr_6$, the product of yield times mobility, $\varphi\Sigma\mu$ is above 1 cm^2 V^{-1} s^{-1}. Because of the limited response time of our system, part of the photoinduced charge carriers might already have recombined which could lead to a substantial lower yield, φ. Moreover, we proposed a model describing the kinetic processes that follow on photogeneration of charge carriers both close the surface and in the bulk of the material. The temperature- and intensity-dependence of the lifetime of mobile charges in the bulk has been explained in terms of shallow electron and hole trap states in the bandgap of the material. Although these traps are present in large amounts, they are energetically shallow. Trap-assisted recombination of charges in the bulk appears to be slow as evidenced by the observation of mobile charges several microseconds after excitation. These results are promising for application in photovoltaics. In agreement with previous TRPL measurements,[14] our results confirm that the recombination of charges at surface states is fast in $Cs_2AgBiBr_6$ and that it becomes the dominant recombination pathway in thin films.

Greul et al.[19] recently demonstrated a photovoltaic device with $Cs_2AgBiBr_6$ as the absorber, with a power conversion efficiency close to 2.5%.[20] Although this confirms the potential of lead-free double perovskites as absorbers, the low efficiency is likely due to fast carrier recombination at the film surface. We therefore propose that future research on $Cs_2AgBiBr_6$ and similar materials should focus on surface passivation to reduce the surface traps and realize the long carrier lifetimes needed for their application in efficient photovoltaic devices.

ASSOCIATED CONTENT

Supporting Information

The Supporting Information is available free of charge on the ACS Publications website at DOI: 10.1021/acs.jpcc.8b00572.

Calculation of the equilibrium distributions of electrons and holes and additional data (PDF)

AUTHOR INFORMATION

Corresponding Authors

*E-mail: d.bartesaghi@tudelft.nl. Phone: 0031(0)152783460 (D.B.).

*E-mail: t.j.savenije@tudelft.nl. Phone: 0031(0)152786537 (T.J.S.).

ORCID

Davide Bartesaghi: 0000-0002-7467-269X

Ferdinand C. Grozema: 0000-0002-4375-799X

Hemamala I. Karunadasa: 0000-0003-4949-8068

Tom J. Savenije: 0000-0003-1435-9885

Notes

The authors declare no competing financial interest.

ACKNOWLEDGMENTS

This research was carried out under project number F71.4.15562a in the framework of the Partnership Program of the Materials innovation institute M2i (www.m2i.nl) and the Foundation of Fundamental Research on Matter (FOM) (www.fom.nl), which is part of the Netherlands Organisation

DOI: 10.1021/acs.jpcc.8b00572
J. Phys. Chem. C 2018, 122, 4809−4816

for Scientific Research (www.nwo.nl). Work by A.H.S. and H.I.K. was supported by the SLAC National Accelerator Laboratory. Part of the research leading to these results has received funding from the European Research Council Horizon 2020 ERC grant agreement no. 648433. The authors acknowledge Eline M. Hutter for critical reading of the manuscript.

REFERENCES

(1) Kojima, A.; Teshima, K.; Shirai, Y.; Miyasaka, T. Organometal Halide Perovskites as Visible-Light Sensitizers for Photovoltaic Cells. *J. Am. Chem. Soc.* **2009**, *131*, 6050−6051.
(2) National Renewable Energy Laboratory. Research Cell Record Efficiency Chart. https://www.nrel.gov/pv/assets/images/efficiency-chart.png (accessed January 25, 2018).
(3) Babayigit, A.; Ethirajan, A.; Muller, M.; Conings, B. Toxicity of Organometal Halide Perovskite Solar Cells. *Nat. Mater.* **2016**, *15*, 247−251.
(4) Filip, M. R.; Giustino, F. Computational Screening of Homovalent Lead Substitution in Organic-Inorganic Halide Perovskites. *J. Phys. Chem. C* **2016**, *120*, 166−173.
(5) Feng, J.; Xiao, B. Effective Masses and Electronic and Optical Properties of Nontoxic $MASnX_3$ (X = Cl, Br and I) Perovskite Structures as Solar Cell Absorber: A Theoretical Study Using HSE06. *J. Phys. Chem. C* **2014**, *118*, 19655−19660.
(6) Umari, P.; Mosconi, E.; De Angelis, F. Relativistic GW Calculations on $CH_3NH_3PbI_3$ and $CH_3NH_3SnI_3$ Perovskites for Solar Cell Applications. *Sci. Rep.* **2014**, *4*, 4467.
(7) Pazoki, M.; Jacobsson, T. J.; Hagfeldt, A.; Boschloo, G.; Edvinsson, T. Effect of Metal Cation Replacement on the Electronic Structure of Metalorganic Halide Perovskites: Replacement of Lead with Alkaline-Earth Metals. *Phys. Rev. B* **2016**, *93*, 144105.
(8) Huang, T. J.; Thiang, Z. X.; Yin, X.; Tang, C.; Qi, G.; Gong, H. $(CH_3NH_3)_2PdCl_4$: A Compound with Two-Dimensional Organic-Inorganic Layered Perovskite Structure. *Chem.—Eur. J* **2016**, *22*, 2146−2152.
(9) Cortecchia, D.; Dewi, H. A.; Yin, J.; Bruno, A.; Chen, S.; Baikie, T.; Boix, P. P.; Grätzel, M.; Mhaisalkar, S.; Soci, C.; Mathews, N. Lead-Free $MA_2CuCl_xBr_{4-x}$ Hybrid Perovskites. *Inorg. Chem.* **2016**, *55*, 1044−1052.
(10) Stoumpos, C. C.; Frazer, L.; Clark, D. J.; Kim, Y. S.; Rhim, S. H.; Freeman, A. J.; Ketterson, J. B.; Jang, J. I.; Kanatzidis, M. J. Hybrid Germanium Iodide Perovskite Semiconductors: Active Lone Pairs, Structural Distortions, Direct and Indirect Energy Gaps, and Strong Nonlinear Optical Properties. *J. Am. Chem. Soc.* **2015**, *137*, 6804−6819.
(11) Jacobsson, T. J.; Pazoki, M.; Hagfeldt, A.; Edvinsson, T. Goldschmidt's Rules and Strontium Replacement in Lead Halogen Perovskite Solar Cells: Theory and Preliminary Experiments on $CH_3NH_3SrI_3$. *J. Phys. Chem. C* **2015**, *119*, 25673−25683.
(12) Morss, L. R.; Siegal, M.; Stenger, L.; Edelstein, N. Preparation of Cubic Chloro Complex Compounds of Trivalent Metals: Cs2NaMCl6. *Inorg. Chem.* **1970**, *9*, 1771−1775.
(13) McClure, E. T.; Ball, M. R.; Windl, W.; Woodward, P. M. Cs_2AgBiX_6 (X = Br, Cl): New Visible Light Absorbing, Lead-Free Halide Perovskite Semiconductors. *Chem. Mater.* **2016**, *28*, 1348−1354.
(14) Slavney, A. H.; Hu, T.; Lindenberg, A. M.; Karunadasa, H. I. A Bismuth-Halide Double Perovskite with Long Carrier Recombination Lifetime for Photovoltaic Applications. *J. Am. Chem. Soc.* **2016**, *138*, 2138−2141.
(15) Volonakis, G.; Filip, M. R.; Haghighirad, A. A.; Sakai, N.; Wenger, B.; Snaith, H. J.; Giustino, F. Lead-Free Halide Double Perovskites via Heterovalent Substitution of Noble Metals. *J. Phys. Chem. Lett.* **2016**, *7*, 1254−1259.
(16) Filip, M. R.; Hillman, S.; Haghighirad, A. A.; Snaith, H. J.; Giustino, F. Band Gaps of the Lead-Free Halide Double Perovskites $Cs_2BiAgCl_6$ and $Cs_2BiAgBr_6$ from Theory and Experiment. *J. Phys. Chem. Lett.* **2016**, *7*, 2579−2585.
(17) Xiao, Z.; Meng, W.; Wang, J.; Yan, Y. Thermodynamic Stability and Defect Chemistry of Bismuth-Based Lead-Free Double Perovskites. *ChemSusChem* **2016**, *9*, 2628−2633.
(18) Savory, C. N.; Walsh, A.; Scanlon, D. O. Can Pb-Free Halide Double Perovskites Support High-Efficiency Solar Cells? *ACS Energy Lett.* **2016**, *1*, 949−955.
(19) Greul, E.; Petrus, M. L.; Binek, A.; Docampo, P.; Bein, T. Highly Stable, Phase Pure $Cs_2AgBiBr_6$ Double Perovskite Thin Films for Optoelectronic Applications. *J. Mater. Chem. A* **2017**, *5*, 19972−19981.
(20) Pan, W.; Wu, H.; Luo, J.; Deng, Z.; Ge, C.; Chen, C.; Jiang, X.; Yin, W.-Y.; Niu, G.; Zhu, L.; et al. $Cs_2AgBiBr_6$ Single-Crystal X-ray Detectors with a Low Detection Limit. *Nat. Photonics* **2017**, *11*, 726−732.
(21) Slavney, A. H.; Leppert, L.; Bartesaghi, D.; Gold-Parker, A.; Toney, M. F.; Savenije, T. J.; Neaton, J. B.; Karunadasa, H. I. Defect-Induced Band-Edge Reconstruction of a Bismuth-Halide Double Perovskite for Visible-Light Absorption. *J. Am. Chem. Soc.* **2017**, *139*, 5015−5018.
(22) Zhou, H.; Chen, Q.; Li, G.; Luo, S.; Song, T.-B.; Duan, H.-S.; Hong, Z.; You, J.; Liu, Y.; Yang, Y. Interface Engineering of Highly Efficient Perovskite Solar Cells. *Science* **2014**, *345*, 542−546.
(23) De Quilettes, D. W.; Vorpahl, S. M.; Stranks, S. D.; Nagaoka, H.; Eperon, G. E.; Ziffer, M. E.; Snaith, H. J.; Ginger, D. S. Impact of Microstructure on Local Carrier Lifetime in Perovskite Solar Cells. *Science* **2015**, *348*, 683−686.
(24) Savenije, T. J.; Ferguson, A. J.; Kopidakis, N.; Rumbles, G. Revealing the Dynamics of Charge Carriers in Polymer:Fullerene Blends Using Photoinduced Time-Resolved Microwave Conductivity. *J. Phys. Chem. C* **2013**, *117*, 24085−24103.
(25) Warman, J. M.; Gelinck, G. H.; de Haas, M. P. The Mobility and Relaxation Kinetics of Charge Carriers in Molecular Materials Studied by Means of Pulse-Radiolysis Time-Resolved Microwave Conductivity: Dialkoxy-Substituted Phenylene-Vinylene Polymers. *J. Phys.: Condens. Matter* **2002**, *14*, 9935−9954.
(26) Warman, J. M.; de Haas, M. P.; Dicker, G.; Grozema, F. C.; Piris, J.; Debije, M. G. Charge Mobilities in Organic Semiconducting Materials Determined by Pulse-Radiolysis Time-Resolved Microwave Conductivity: π-Bond Conjugated Polymers Versus π-π-Stacked Discotics. *Chem. Mater.* **2004**, *16*, 4600−4609.
(27) Gélvez-Rueda, M. C.; Cao, D. H.; Patwardhan, S.; Renaud, N.; Stoumpos, C. C.; Schatz, G. C.; Hupp, J. T.; Farha, O. K.; Savenije, T. J.; Kanatzidis, M. G.; et al. Effect of Cation Rotation on Charge Dynamics in Hybrid Lead Halide Perovskites. *J. Phys. Chem. C* **2016**, *120*, 16577−16585.
(28) Klein-Kedem, N.; Cahen, D.; Hodes, G. Effect of Light and Electron Beam Irradiation on Halide Perovskites and Their Solar Cells. *Acc. Chem. Res.* **2016**, *49*, 347−354.
(29) Herz, L. M. Charge-Carrier Mobilities in Metal Halide Perovskites: Fundamental Mechanisms and Limits. *ACS Energy Lett.* **2017**, *2*, 1539−1548.
(30) Bi, Y.; Hutter, E. M.; Fang, Y.; Dong, Q.; Huang, J.; Savenije, T. J. Charge Carrier Lifetimets Exceeding 15 μs in Methylammonium Lead Iodide Single Crystals. *J. Phys. Chem. Lett.* **2016**, *7*, 923−928.
(31) Savenije, T. J.; Ponseca, C. S., Jr.; Kunneman, L.; Abdellah, M.; Zheng, K.; Tian, Y.; Zhu, Q.; Canton, S. E.; Scheblykin, I. G.; Pullerits, T.; et al. Thermally Activated Exciton Dissociation and Recombination Control the Carrier Dynamics in Organometal Halide Perovskite. *J. Phys. Chem. Lett.* **2014**, *5*, 2189−2194.
(32) Milot, R. L.; Eperon, G. E.; Snaith, H. J.; Johnston, M. B.; Herz, L. M. Temperature-Dependent Charge-Carrier Dynamics in $CH_3NH_3PbI_3$ Perovskite Thin Films. *Adv. Funct. Mater.* **2015**, *25*, 6218−6227.
(33) Brenner, T. M.; Egger, D. A.; Kronik, L.; Hodes, G.; Cahen, D. Hybrid Organic-Inorganic Perovskites: Low-Cost Semiconductors with Intriguing Charge-Transport Properties. *Nat. Rev. Mater.* **2016**, *1*, 15007.

DOI: 10.1021/acs.jpcc.8b00572
J. Phys. Chem. C 2018, 122, 4809−4816

(34) Hutter, E. M.; Eperon, G. E.; Stranks, S. D.; Savenije, T. J. Charge Carriers in Planar and Meso-Structured Organic-Inorganic Perovskites: Mobilities, Lifetimes, and Concentrations of Trap States. *J. Phys. Chem. Lett.* **2015**, *6*, 3082−3090.

DOI: 10.1021/acs.jpcc.8b00572
J. Phys. Chem. C 2018, 122, 4809−4816